

Multi-physics constraints at different densities to probe nuclear symmetry energy in hyperonic neutron stars

Suprovo Ghosh 1 , Bikram Keshari Pradhan 1 , Debarati Chatterjee 1,* , Jürgen Schaffner-Bielich 2

¹ Inter-University Centre for Astronomy and Astrophysics, Pune University Campus, Pune - 411007, India

² Institut für Theoretische Physik, Goethe Universität, Max von Laue-Straße 1, 60438 Frankfurt am Main, Germany

Correspondence*: Corresponding Author debarati@iucaa.in

ABSTRACT

The appearance of strangeness in the form of hyperons within the inner core of neutron stars is expected to affect its detectable properties such as its global structure or gravitational wave emission. In this work, we explore the parameter space of hyperonic stars within the framework of the Relativistic Mean Field model allowed by present uncertainties in state-of-the-art nuclear and hypernuclear experimental data. We impose multi-physics constraints at different density regimes to restrict the parameter space: Chiral effective field theory, heavy-ion collision data as well as multi-messenger astrophysical observations of neutron stars. We investigate possible correlations between empirical nuclear and hypernuclear parameters, particularly the symmetry energy and its slope, with observable properties of neutron stars. We do not find a correlation for the hyperon parameters and the astrophysical data. However, the inclusion of hyperons generates a tension between the astrophysical and heavy ion data constraining considerable the available parameter space.

Keywords: symmetry energy, hyperons, neutron stars, equation of state, nuclear, hypernuclear, heavy-ion, multi-messenger

Abstract length: 149 words Manuscript length: 5435 Number of Figures: 13 Number of Tables: 1

1 INTRODUCTION

Understanding strong interaction among hadrons is one of the most intriguing topics in nuclear physics. Despite the recent progress in understanding the phase diagram of Quantum Chromodynamics (QCD), the theory of strong interactions [1, 2], we are still far from achieving a unified description of nuclear matter under extreme conditions of density and temperature. While terrestrial nuclear experiments probe densities close to nuclear saturation density ($n_0 \sim 0.16 \text{ fm}^{-3}$) [3, 4], heavy-ion collision (HIC) experiments [5, 6]

provide information about hot and dense matter at several times n_0 . Recent progress in Lattice QCD [7, 8, 9] are also providing new constraints on the properties of matter at high temperature and low densities. Neutron stars, on the other hand, are astrophysical laboratories that provide us an opportunity to investigate ultrahigh density (up to 10 times n_0) and low temperature regime of the QCD phase diagram, given the conditions that exist only in its interior [10, 11].

Strangeness adds a new dimension to the description of nuclear matter. The presence of strangeness has already been established in heavy-ion collisions (appearance of hyperons and kaons) or in finite nuclear systems (hypernuclei). It is also conjectured that strangeness containing matter, in the form of hyperons, kaons or even deconfined quark matter, can appear at the ultra-high densities that exist in the core of a neutron star (NS). The appearance of strangeness can have significant impact on NS composition, structure and observable astrophysical properties, such as its mass, radius, cooling or gravitational wave (GW) emission [12].

In order to connect the NS internal composition with its global properties, one requires an Equation of State (EoS) [13, 3, 1]. The theoretical description of NS matter therefore requires the construction of models of hadron-hadron interaction, using non-relativistic (such as Skyrme or Gogny interactions) [14, 15, 16] or relativistic (Relativistic Mean Field or Dirac-Brueckner-Hartree-Fock methods) [17, 18] techniques. In the case of microscopic models (such as Brueckner-Hartree-Fock method), the interactions are rigorously calculated from lowest order term to increasing order. But the poor knowledge of three-nucleon forces limits their applicability to reproduce real astrophysical data. Phenomenological models are more successful, with the model parameters usually constrained at densities close to n_0 and low values of isospin (neutron-proton ratio), but the uncertainty increases at larger densities and asymmetries. The nuclear symmetry energy (the difference between the binding energies of symmetric nuclear matter and neutron matter) is a key quantity that governs the difference in the behaviour of infinite symmetric nuclear matter and neutron star matter.

Neutron stars are particularly interesting, as they can be observed via electromagnetic (X-ray, γ -ray, radio waves) as well as gravitational waves, opening up a new era of multi-messenger astronomy. Electromagnetic multi-wavelength observations of NSs reveal a wealth of details about its global structure [19, 20]. NS masses can be determined to high precision using post-Keplerian effects in NSs in binary [21]. Traditionally radius measurements from thermal emission suffered from large uncertainties [22, 23, 24], but the recently launched NICER (Neutron Star Interior Composition Explorer) [25, 26, 27, 28, 29] mission has improved NS estimates by exploiting a novel scheme of modulation profiles of pulses. Finally with the recent detection of GWs for the first time from NS-NS (GW170817) [30], NS-BH (GW200105 and GW200115) [31] and GW190425 [32] systems by LIGO [33] and Virgo [34], GW astronomy is allowing us to probe directly the interior of NSs. The tidal deformation of NSs in the strong gravitational field of its binary companion measured during the inspiral phase of the merger depends on the EoS, and therefore reveals information about its radius and interior composition [35, 36, 37, 38].

In the recent past, there have been several attempts to impose constraints on the NS EoS by using data from NS multi-messenger astrophysical observations within a statistical Bayesian scheme [39, 40, 41, 42, 43, 44, 45]. In such a scheme, the low density EOS constrained by theoretical and experimental nuclear physics is matched with parametrized high density EOSs satisfying gravitational wave and electromagnetic data [46, 47, 48, 49, 50]. Usually the EoSs are based on different parametrization

schemes such as piecewise polytropes [38, 51, 52, 53], spectral representation [54, 55], speed-of-sound parametrization [47, 56, 57] or nuclear meta-modelling technique [58]. Only a few recent works used the RMF model [59] or hybrid (nuclear + piecewise polytope) parametrizations [41] to obtain posterior distributions of empirical parameters. Correlations among empirical nuclear parameters and some chosen NS observables have only recently been explored [60, 61, 62, 63]. Although several of these works suggested probing the effect of the presence of hyperons, none of them consistently included hyperons within such a scheme. It therefore remains to be investigated whether one can restrict the parameter space of uncertainties associated with hyperons (hypernuclear potentials or hyperon couplings) or if they show any physical correlations with measurable properties such as nuclear saturation parameters or NS astrophysical observables.

In a recent work [64], multi-physics constraints were imposed at different density regimes on the nuclear EoS using a "cut-off scheme", and correlations of nuclear saturation parameters with astrophysical observables were investigated. Motivated by the Bayesian approach, the parameters of the realistic nuclear model were varied within their allowed uncertainties, compatible with state-of-the-art nuclear experimental data and the parameter space constrained using a combination of current best-known physical constraints at different density regimes: theoretical (chiral effective field theory) at low densities, multi-messenger (multi-wavelength electromagnetic as well as GW) astrophysical data at high densities and experimental (nuclear and heavy-ion collision) at intermediate densities [65, 66] to restrict the parameter space of the nuclear model. Further, nuclear and heavy-ion collision experiments are isospin symmetric (same number of neutrons and protons), so studying NS matter provides information about the unknown nuclear symmetry energy.

In this article, we extend the above investigation to neutron star matter including strangeness, particularly hyperons. Within the framework of the RMF model, and allowing for a parameter space spanning current uncertainties in nuclear and hypernuclear physics, we impose multi-physics constraints in different density regimes from terrestrial nuclear/hypernuclear and multi-messenger astrophysical data. The aim of this study is to investigate possible correlations between empirical nuclear and hypernuclear parameters (particularly the symmetry energy and its slope) with NS astrophysical observables.

The structure of the article is as follows: in Sec. 2, we describe the methods used to determine the composition of NS matter including hyperons in the framework of the RMF model. In Sec. 3, we impose constraints at different densities on the hyperonic EoS. In Sec. 4, we discuss the results of this investigation and in Sec. 5 we discuss the implications of these findings.

2 METHODS

As discussed in Sec. 1, we calculate the beta equilibrated, charge-neutral NS EoS within the RMF framework. For our investigation, we consider the standard baryon octet as well as electrons and muons. The interaction Lagrangian density (\mathcal{L}) considered in this work is given in Eq. 1 [67, 68]. In this model, the baryon-baryon interaction is mediated by the exchange of scalar (σ), vector (ω), isovector (ρ) mesons, and the strange baryon, i.e., hyperon-hyperon interactions are carried out by additional strange scalar (σ *)

and strange vector (ϕ) mesons.

$$\mathcal{L} = \sum_{B} \bar{\psi}_{B} \Big(i \gamma^{\mu} \partial_{\mu} - m_{B} + g_{\sigma B} \sigma - g_{\omega B} \gamma_{\mu} \omega^{\mu} - g_{\rho B} \gamma_{\mu} \vec{I}_{B} \cdot \vec{\rho}^{\mu} \Big) \psi_{B} + \frac{1}{2} (\partial_{\mu} \sigma \partial^{\mu} \sigma - m_{\sigma}^{2} \sigma^{2}) - U_{\sigma} \\
+ \frac{1}{2} m_{\omega}^{2} \omega_{\mu} \omega^{\mu} - \frac{1}{4} \omega_{\mu\nu} \omega^{\mu\nu} - \frac{1}{4} (\vec{\rho}_{\mu\nu} \cdot \vec{\rho}^{\mu\nu} - 2m_{\rho}^{2} \vec{\rho}_{\mu} \cdot \vec{\rho}^{\mu}) + \Lambda_{\omega} (g_{\rho N}^{2} \vec{\rho}_{\mu} \cdot \vec{\rho}^{\mu}) (g_{\omega N}^{2} \omega_{\mu} \omega^{\mu}) \\
+ \sum_{Y} \bar{\psi}_{Y} (g_{\sigma^{*}Y} \sigma^{*} - g_{\phi Y} \gamma_{\mu} \phi^{\mu}) \psi_{Y} + \frac{1}{2} m_{\phi}^{2} \phi_{\mu} \phi^{\mu} - \frac{1}{4} \phi_{\mu\nu} \phi^{\mu\nu} + \frac{1}{2} (\partial_{\mu} \sigma^{*} \partial^{\mu} \sigma^{*} - m_{\sigma^{*}}^{2} \sigma^{*2}) \\
+ \sum_{\ell = \{e^{-}, \mu^{-}\}} \bar{\psi}_{\ell} (i \gamma^{\mu} \partial_{\mu} - m_{\ell}) \psi_{\ell} \tag{1}$$

where,

$$U_{\sigma} = \frac{1}{3}bm_N(g_{\sigma N}\sigma)^3 + \frac{1}{4}c(g_{\sigma N}\sigma)^4$$

In Eq. 1, B stands for the baryon octet $(p, n, \Lambda, \Sigma^-, \Sigma^0, \Sigma^+, \Xi^-, \Xi^0)$ whereas Y stands for hyperons $(\Lambda, \Sigma^-, \Sigma^0, \Sigma^+, \Xi^-, \Xi^0)$. One can solve the equation of motion governing constituent particle fields (Ψ) as well as those of mesons following [69, 68]. Replacing the meson fields with their mean values in RMF framework, the energy density (ϵ) corresponding to the Lagrangian given in Eq. 1 can be expressed as,

$$\epsilon = \frac{1}{2}m_{\sigma}^{2}\bar{\sigma}^{2} + \frac{1}{2}m_{\omega}^{2}\bar{\omega}^{2} + \frac{1}{2}m_{\rho}^{2}\bar{\rho}^{2} + \frac{1}{2}m_{\sigma^{*}}^{2}\bar{\sigma}^{*2} + \frac{1}{2}m_{\phi}^{2}\bar{\phi}^{2} + \frac{1}{3}bm_{N}(g_{\sigma N}\bar{\sigma})^{3} + \frac{1}{4}c(g_{\sigma N}\bar{\sigma})^{4}
+ 3\Lambda_{\omega}(g_{\rho N}g_{\omega N}\bar{\rho}\bar{\omega})^{2} + \sum_{B}\frac{g_{sB}}{2\pi^{2}}\int_{0}^{k_{FB}}\sqrt{k^{2} + m_{B}^{*2}}dk + \sum_{\ell}\frac{g_{s\ell}}{2\pi^{2}}\int_{0}^{k_{F\ell}}\sqrt{k^{2} + m_{\ell}^{2}}dk \quad (2)$$

Where g_{si} and k_{Fi} represent the spin degeneracy and Fermi momentum of the 'ith' species respectively. The baryon effective mass (m_B^*) is then defined as $m_B^* = m_B - g_{\sigma B}\bar{\sigma} - g_{\sigma^*B}\bar{\sigma}^*$. The pressure can be expressed using Gibbs-Duhem relation,

$$p = \sum_{i=B,\ell} \mu_i n_i - \epsilon \tag{3}$$

with n_i being the number density of i^{th} constituent. The chemical potentials for baryon (μ_B) and lepton (μ_ℓ) are given by,

$$\mu_{B} = \sqrt{k_{FB}^{2} + m_{B}^{*2}} + g_{\omega_{B}}\bar{\omega} + g_{\phi_{B}}\bar{\phi} + I_{3_{B}}g_{\rho_{B}}\bar{\rho}$$

$$\mu_{\ell} = \sqrt{k_{F\ell}^{2} + m_{\ell}^{2}}.$$
(4)

2.1 Nucleonic matter

The isoscalar nucleon-meson coupling parameters $(g_{\sigma N}, g_{\omega N}, b, \text{ and } c)$ are determined by fixing the nuclear saturation parameters: nuclear saturation density (n_0) , binding energy per nucleon at saturation (E_{sat}) , incompressibility (K_{sat}) and the effective nucleon mass (m^*) at saturation. On the other hand the

isovector couplings ' $g_{\rho N}$ ' and ' Λ_{ω} ' are fixed to the symmetry energy (E_{sym}) and slope of symmetry energy (L_{sym}) at saturation [69, 70, 64]. The range of empirical parameters considered in this work are consistent with state-of-the-art nuclear experimental data [64] and are summarised in Table. 1.

2.2 Hyperonic matter

In the Lagrangian (Eq. 1), the attractive interaction among hyperons is meditated by the exchange of strange scalar (σ^*) meson and the repulsive interaction is mediated by exchange of strange vector (ϕ) meson. However, it has been concluded that models with attractive hyperon-hyperon interaction show incompatibility with observations of the maximum NS mass [67]. Hence we set the strange scalar couplings to 0, i.e, $g_{\sigma Y} = 0$ and the remaining non-strange hyperon meson coupling constants ($g_{\sigma Y}$) are fitted to the hyperon-nucleon potential (U_Y) at saturation using Eq. 5 [67]. Among the nucleon-hyperon potentials, the best known potential is that of the hyperon Λ , having a value of $U_{\Lambda} = -30$ MeV [71, 72]. Although the potential depths for hyperons Σ and Ξ are not known precisely, it has been concluded that the Σ -nucleon potential is repulsive [73, 74, 75] whereas U_{Ξ} is attractive in nature [76, 77, 74]. Hence for this investigation we vary U_{Σ} in the range of 0 to +30 MeV and U_{Ξ} from -30MeV to 0. The vector hyperon couplings ($g_{\omega Y}, g_{\phi Y}$) are fixed to their SU(6) values (see Eq. 6) [78, 67].

$$U_Y(n_0) = -g_{\sigma Y}\bar{\sigma} + g_{\omega Y}\bar{\omega} \tag{5}$$

$$g_{\omega\Lambda} = g_{\omega\Sigma} = 2g_{\omega\Xi} = \frac{2}{3}g_{\omega N}$$

$$2g_{\phi\Lambda} = 2g_{\phi\Sigma} = g_{\phi\Xi} = \frac{-2\sqrt{2}}{3}g_{\omega N}$$
(6)

Recent lattice QCD calculations by the HALQCD group extracted hyperon potentials at almost physical quark masses and used it to estimate the hyperon potentials in pure neutron matter and in nuclear matter by using the Brueckner-Hartree-Fock approximation [7, 8]. They find that the hyperon potentials in nuclear matter are $U_{\Lambda}=-28~{\rm MeV},~U_{\Sigma}=+15{\rm MeV}$ and $U_{\Xi}=-4~{\rm MeV}$. From their figure 4 in [8] one can read off the hyperon potentials for Σ^- and Σ^+ , as well as for Ξ^0 and Ξ^- in pure neutron matter. The relevant for neutron star matter are the ones for the Σ^- and the Ξ^- with the potentials of +25 MeV and + 6 MeV, respectively. However, these results suggest that the isovector hyperon coupling $(g_{\rho Y})$ differs from its SU(6) quark model values. Where the isospin potential for the Ξ would be as large as the one for nucleons and the one for the Σ even twice as large. For a typical nucleon isospin potential of about 32 MeV one arrives at hyperon isospin potentials which are more than a factor two larger than the ones from the HALQCD analysis. We therefore introduce a scaling parameter 'y,' which ranges from 0 to 1 (0 to SU(6) coupling strength) to span the uncertainty in the hyperon-isovector coupling. In that case, $g_{\rho Y}$ can be expressed as,

$$g_{\rho\Lambda} = 0$$

$$\frac{g_{\rho\Xi}}{g_{\rho N}} = \frac{1}{2} \frac{g_{\rho\Sigma}}{g_{\rho N}} = y, \quad y \in [0, 1].$$
(7)

The effect of the variation in the y-parameter (isovector hyperon coupling) on the particle fractions can be understood from Fig. 1. For a chosen parameter set from Table 1, Ξ^- starts to appear at 2.27, 2.34 and 2.45 n_0 for y values 0, 0.5 and 1 respectively. However Ξ^0 starts to appear 6.977, 6.943 and

 $6.850 n_0$ for y changing from 0 to 1 in steps of 0.5. One must note that the threshold of appearance of the hyperons will depend upon the hyperon potentials and the nuclear saturation parameters chosen for the EoS.

2.3 Global structure

The equilibrium structure of a non-rotating, relativistic NS is obtained by solving the coupled equations of hydrostatic equilibrium known as the Tolman-Oppenheimer-Volkof (TOV) equations [10, 79]

$$\frac{dm(r)}{dr} = 4\pi\varepsilon(r)r^{2},$$

$$\frac{dp(r)}{dr} = -\frac{[p(r) + \varepsilon(r)][m(r) + 4\pi r^{3}p(r)]}{r(r - 2m(r))},$$
(8)

With the given equation of state which gives a relation between the energy density (ε) and pressure (p), these TOV equations (8) are integrated from the centre of the star to the surface with the boundary conditions of vanishing mass, $m|_{r=0}=0$, at the centre of the star, and a vanishing pressure, $p|_{r=R}=0$, at the surface. Varying the central density for a given EoS, we can get a sequence of NSs with different mass and radius, thus giving the M-R curves.

The tidal deformability parameter quantifies the degree of the tidal deformation effects due to the companion in coalescing binary NS systems during the early stages of an inspiral. It is defined as:

$$\lambda = -\frac{Q_{ij}}{\varepsilon_{ij}} \tag{9}$$

where Q_{ij} is the induced mass quadrupole moment of the NS and ε_{ij} is the gravitational tidal field of the companion. The tidal deformability λ is related to the dimensionless l=2 tidal Love number k_2 as [80, 81].

$$\Lambda = \frac{2}{3}k_2 \left(\frac{R}{M}\right)^5 \,, \tag{10}$$

The tidal Love number (k_2) can be obtained by solving a set of differential equations coupled with the TOV equations [82]. The total tidal effect of two neutron stars in an inspiraling binary system is given by the mass-weighted (dimensionless) tidal deformability $\tilde{\Lambda}$ defined as [83]

$$\tilde{\Lambda} = \frac{16}{13} \frac{(M_1 + 12M_2)M_1^4 \Lambda_1 + (M_2 + 12M_1)M_2^4 \Lambda_2}{(M_1 + M_2)^5}$$
(11)

where $\Lambda_1 = \Lambda_1(M_1)$ and $\Lambda_2 = \Lambda_2(M_2)$ are the (dimensionless) tidal deformabilities and M_1, M_2 are the masses of the individual binary components respectively.

3 MULTI-DENSITY CONSTRAINTS

In this work, we constrain the parameter space of the nucleonic and hyperonic matter as described in Sec. 2 using a "cut-off filter" scheme where we impose strict limits from nuclear and astrophysical observation to

obtain the posteriors. In the language of Bayesian analysis, the priors are obtained by varying the nuclear empirical parameters, hyperon potentials and isovector couplings uniformly within their uncertainty range in Table 1 and the likelihood functions are appropriately chosen physical conditions as Filter functions described in Sec. 3.1.

In Miller et al. (2019) [84], they pointed out the statistical uncertainties in constraining EoS by putting strict limits from multi-messenger observations of neutron stars like we have used here. With a very large number of priors, this cut-off scheme gives a correct estimate of the nuclear parameter ranges consistent with the observations. Recent works [38, 37, 85, 86, 87] also used similar cut-off schemes for constraining the EoS of ultra-dense matter. In the recent work by Ghosh et al. [64], it was explicitly shown that including the statistical re-weighting using χ -squared statistics might change the posterior probability distribution slightly, but it does not significantly alter the physical correlation between nuclear empirical parameters and astrophysical observables. So, we adopt this "cut-off filter" scheme for this work.

3.1 Filter functions

The following physical constraints at different densities from multi-disciplinary physics are applied in this work -

• at low densities: χEFT

Chiral EFT is an effective theory of QCD that describes strong many-body interactions among nucleons using order by order expansions in terms of contact interactions and long-range pion exchange interactions. In particular, the χ EFT expansion gives estimates of theoretical uncertainties depending on local chiral two and three-nucleon interactions using quantum Monte Carlo methods, which are one of the most precise many-body methods for nuclear physics [88, 89]. The EoS of pure neutron matter (PNM) can be well constrained at low baryon densities n_b in the range of \sim 0.5-1.4 n_0 [90].

• at high densities: NS astrophysical data

The constraints on the EoS at high density come from multi-messenger astrophysical observations, such as high mass NS observations, GW measurement of tidal deformability from binary neutron star mergers as follows:

- 1. From the recent observations of the heaviest known pulsar PSR J0740+6620, the maximum mass of the neutron stars should be equal to or exceed $2.08^{+0.07}_{-0.07}~M_{\odot}$ [91]. This sets an upper bound on the maximum NS masses corresponding to the EoSs considered.
- 2. The recent analyses of the GW170817 event [36] apply a constraint on the upper bound of the effective tidal deformability $\tilde{\Lambda} < 720$ [92] using the low-spin highest posterior density interval for tidal deformability. We do not consider the lower limit on tidal deformability in this study. As explained in Sec. 2.3, the tidal deformability depends on the mass and radius (see Eq. 10), and therefore this result also leads to a constraint on the mass-radius relation [37, 38].

• at intermediate densities: heavy ion collision experiments

Heavy-ion collision experiments can provide additional information about the behaviour of hot dense matter at intermediate densities $\sim 1-3n_0$. As in our previous investigation [64], we impose constraints from three different heavy-ion collision experiments:

- 1. **KaoS experiment :** Subthreshold K^+ meson production in Au+Au & C+C nuclear collisions at the Kaon Spectrometer (KaoS) experiment at GSI, Darmstadt [93] yield kaon multiplicity, which is an indicator of the compressibility of dense matter at densities $\sim 2-3n_0$. The analysis of the experimental data using Isospin Quantum Molecular Dynamics (IQMD) transport models points towards a soft EoS [93, 94] and can be described by a simple Skyrme ansatz with an incompressibility $\lesssim 200$ MeV. The constraint given by the KaoS data implies only those nucleon potentials which are more attractive than the Skyrme parametrization within the considered density regime will be allowed.
- 2. **FOPI experiment :** Elliptic flow data in Au+Au collisions between 0.4 and 1.5A GeV by the FOPI collaboration [5], provides constraints for the EoS of compressed symmetric nuclear matter (SNM). Analysing the FOPI data using IQMD transport codes, one can obtain a constraint for the binding energy of SNM in the density region of $n_b/n_0 \sim 1.4-2.0$ [5]. To impose this constraint, the binding energy for SNM is calculated for the input parameters, and only permitted if they lie inside the band allowed by the FOPI data in this density range.
- 3. **ASY-EOS experiment :** Information about the symmetry energy for ANM at supra-saturation densities can be obtained from directed and elliptic flows of neutrons and light charged particles measured for the reaction 197 Au+ 197 Au at 400 MeV/nucleon incident energy within the ASY-EOS experimental campaign at the GSI, Germany [6]. To impose the ASY-EOS filter, the symmetry energy of ANM EoS is calculated for the input parameters and allowed only if the symmetry energy lies inside the band allowed by the data in the range of $\sim 1.1 2.0n_0$.

3.2 Correlations

Using the posterior obtained from the analysis, we look for any physical correlation of the nuclear parameters, hyperon potentials, isovector coupling among themselves and also with the astrophysical observables such as the mass and radius of the canonical $1.4M_{\odot}$ and the massive $2M_{\odot}$ NS. For this study, we use Pearson's linear correlation coefficient defined as [95].

$$R_{XY} = \frac{Cov(X,Y)}{\sqrt{Cov(X,X)}\sqrt{Cov(Y,Y)}}$$
(12)

where Cov(X, Y) is the co-variance between two variables X and Y defined as

$$Cov(X,Y) = \frac{1}{N} \sum_{i} (X_i - M(X))(Y_i - M(Y))$$
 (13)

where N is the no. of sample points and M(X) is the mean of the variable X defined as $M(X) = \frac{1}{N} \sum_{i} X_{i}$.

4 RESULTS

4.1 Effect of χ EFT + astro filters

By randomly varying the parameter space of the nuclear parameters and hyperon potentials from Table. 1, we generate the uniformly distributed prior set. After generating the random EoSs, we use the χ EFT and astrophysical filters described in Sec. 3.1 to obtain filtered sets for the parameters and NS observables. For χ EFT, we evaluate the binding energies in the density range of $n_b/n_0 \sim 0.5-1.4$ corresponding to

the χ EFT data and allow only those parameter sets that lie within the band allowed by χ EFT calculations (Fig. 2).

After obtaining the posterior χ EFT, we use the same parameter set to obtain the hyperonic EoS using hyperon potentials and couplings given in Sec. 2.2.We then solve the coupled TOV equations (8)(10) to obtain the mass, radius and tidal deformability of the NSs. Using the multi-messenger astrophysical and GW observation of NSs given in Sec. 3.1, we rule out further combinations of parameter sets and allow only those combinations which simultaneously satisfy all constraints on NS observables. In Fig. 3, we plot the mass-radius relations and the dimensionless tidal deformability as a function of NS mass corresponding to the filtered hyperonic EoSs. We can see that NS radii span a wide range from 11-14 km.

4.2 Correlations

After obtaining the posterior parameter space, we look for any physical correlation among the parameters and the NS observables as well as within themselves. In Fig. 4, we display the correlation matrix of the following quantities: nuclear empirical parameters $(n_0, E_{sat}, K_{sat}, E_{sym}, L_{sym})$, the effective mass m^*/m , hyperon potentials (U_{Σ}, U_{Ξ}) , hyperon-isovector coupling parameter y and the NS observables $(R_{1.4M_{\odot}}, \Lambda_{1.4M_{\odot}}, R_{2M_{\odot}}, \Lambda_{2M_{\odot}})$ after applying both χ EFT and astrophysical observations filter. Some of the main observations from the correlation matrix are listed below:

- n_0 and m^*/m show a high correlation (0.71).
- n_0 has a moderate correlation with the NS observables. The correlation is noticeable (0.54) for the constraints for $1.4M_{\odot}$ NS but is negligible for the constraints for $2 M_{\odot}$.
- Symmetry energy E_{sym} and its slope L_{sym} display a strong correlation (0.79) which only appears when we apply the χ EFT filter. This correlation only comes from the χ EFT filter around saturation density which is in agreement with previous literature [69, 64].
- We see a moderate correlation (0.44) between L_{sym} and effective mass m^*/m after applying the χEFT filter.
- The correlation of m^*/m with the NS observables is pretty low (~ 0.1 for $1.4 M_{\odot}$ and ~ 0.3 for $2.0 M_{\odot}$ stars) which is quite the opposite to the purely nucleonic case [64].
- The correlation between slope of symmetry energy L_{sym} and radius of $1.4 M_{\odot}$ NS is also lower (around 0.4). A correlation between L_{sym} and $R_{1.4 M_{\odot}}$ has been reported in several articles in the literature [96, 97, 98, 99], although recent articles find $R_{1.4 M_{\odot}}$ to be nearly independent of L_{sym} [69, 64].
- All the NS observables (radius and dimensionless tidal deformability for 1.4 M_{\odot} and 2 M_{\odot} NS), as expected, show a strong correlation with each other (according to Eq. 9) although we find a moderate correlation with the observables between 1.4 M_{\odot} and 2 M_{\odot} NSs.
- We did not find any correlation between the hyperon potentials and the isovector coupling parameter y with other nuclear parameters and the astrophysical observables.

To understand the correlations better, in Fig. 5 we plot the posterior distribution of the nuclear parameters $(n_0, E_{sym}, L_{sym} \text{ and } m^*/m)$ which show significant correlations and the astrophysical observables $(R_{1.4M_{\odot}}, R_{2M_{\odot}}, \Lambda_{2M_{\odot}})$ after applying both the χ EFT and the astrophysical constraints.

From the corner plots, we see that after applying the χ EFT filter, both the median values of symmetry energy and its slope L_{sym} shift towards a higher value compared to their prior range in Table. 1 which leads to the strong correlation between them. For the effective mass, we see that the peak is around 0.63

which is lower than we observed for purely nucleonic matter [69, 64]. This is because when we include hyperon, the EoS become softer [68]; so to satisfy the astrophysical constraint of maximum mass above $2M_{\odot}$ and tidal deformability, the posterior of m^*/m shifts towards a lower value. Also, from Fig 5 in [64], we know that χ EFT filter removes parameter sets with low effective mass and slope of symmetry energy which gives rise to a moderate correlation between L_{sym} and m^*/m observed here. For this reason, for the hyperonic case along with χ EFT filter, the range of effective mass becomes narrow and peaks towards a lower value (around 0.63) which indeed restricts the radius of $1.4M_{\odot}$ star to 12.6-13.4 km. This is why we observe a very low correlation between m^*/m and the astrophysical observables. We also conclude that there is no correlation between the hyperon potentials (U_{Σ}, U_{Ξ}) and the NS astrophysical observables.

4.3 Effect of all filters : χ EFT + astro + HIC (KaoS+FOPI+ASY-EOS)

We first generated 50,000 prior sets, and on applying all filters (χ EFT, astrophysical data, HIC) obtained almost no posterior sets. In order to understand the effect of the HIC filters, we then passed the prior sets only through the KaOS, FOPI and ASY-EOS filters and plotted the posterior of each nuclear parameters (see Fig. 6). From the figures, we observe that in the K_{sat} distribution, the values are restricted below 240 MeV after HIC filters, and this is the effect of the KaoS filter. In the L_{sym} distribution, the values are restricted to > 55 MeV after HIC filters, resulting in a decreased correlation between L_{sym} and E_{sym} . Both these effects were observed in nucleonic case also and discussed in our previous paper [64]. The most interesting is the distribution of m^*/m . In Sec.4.2, we noted that including hyperons shifts m^*/m to lower value for astrophysical filters. When we apply HIC filters, we see m^*/m values peak at a higher value around 0.70. The distributions intersect at the two tail ends of the Gaussian curves, giving a very narrow range with low probabilities. This explains why there are so few posterior points due to the combined filters.

In order to obtain a correlation plot after applying all filters, we generated a very large number (2 million) of priors after restricting the prior range to m^*/m to 0.64 - 0.7 and managed to obtain 200 posterior sets. The resulting correlation plot with this set is given in Fig. 7. We see that effects of the HIC filters on correlations are the same as in the nucleonic case [64]: decrease of $L_{sym} - E_{sym}$ correlation, increase of n_0 correlation with NS astrophysical observables and increase of $K_{sat} - m^*/m$ correlation. We checked that allowing for hyperons mean that hyperons appear in all the cases investigated; Λ hyperons always appear close to $2n_0$, while the threshold for appearance of Σ and Ξ hyperons depend on the value of the corresponding hyperon potentials. One may also note that for $1.4 M_{\odot}$ stars, the fraction of hyperons in the core is lower than in more massive $2M_{\odot}$ stars.

5 DISCUSSION

5.1 Summary of present results

The motivation of this study is to investigate any existing correlations between empirical nuclear and hypernuclear parameters (particularly the symmetry energy and its slope) and with NS multi-messenger astrophysical observables such as its mass, radius and tidal deformability. To this aim, we extended our previous investigation [64] from nucleonic to hyperonic matter in NSs, i.e. within the framework of the RMF model, we constrained the parameter space allowed by current uncertainties in nuclear and hypernuclear physics, by imposing multi-physics constraints at different density regimes: chiral effective field theory at low densities, astrophysical constraints at high densities and heavy-ion collision data at

intermediate energies.

First, using the filtered EoSs satisfying constraints from both χ EFT and astrophysical data, we searched for any physical correlation among the parameters and the NS observables as well as among themselves. We found that the effective nucleon mass m^*/m and saturation nuclear density n_0 show strong correlation. We found n_0 to be moderately correlated with radius and tidal deformability of $1.4 M_{\odot}$ NSs, but weakly correlated with those of $2 M_{\odot}$ stars. The correlation of m^*/m with the NS observables was found to be low, contrary to the purely nucleonic case. It is interesting to note that the symmetry energy E_{sym} and its slope L_{sym} showed significant correlation after imposing the χ EFT filter. There is a non-negligible correlation of m^*/m with L_{sym} .

On applying all filters from χ EFT, astrophysical and heavy-ion data, we found that very few nuclear parameter sets are able to satisfy all constraints simultaneously. By monitoring the individual posterior distributions of the nuclear saturation parameters, we confirmed the existence of a "tension" between the constraints from the first two filters with those of heavy-ion data. The values of K_{sat} are restricted to below 240 MeV due to the KaoS constraint and L_{sym} to values larger than 55 MeV, drastically reducing the available parameter space. Further, low values of m^*/m are allowed by astrophysical filters, while heavy-ion data allows large values. The overall effect of applying the heavy-ion filters was found to be same as in the nucleonic case [64]: a decreased $L_{sym}-E_{sym}$ correlation, increased n_0 correlation with NS astrophysical observables and enhanced $K_{sat}-m^*/m$ correlation.

5.2 Comparison with prior research

There are several contrasting results in the hyperonic case as compared with the nucleonic case [64]. Mainly we found a decreased correlation of m^*/m with the NS observables, and an increased correlation of n_0 with m^*/m and NS observables for $1.4M_{\odot}$ NS. Radii and dimensionless tidal deformability (for $1.4M_{\odot}$ and $2M_{\odot}$), show a strong correlation with each other as expected. However we find a moderate correlation with observables of $1.4M_{\odot}$ with $2M_{\odot}$ stars. This is due to the reduced range of radii for hyperonic stars. We checked that the distribution of m^*/m shifts to lower values (peak around 0.63) in posteriors for hyperons compared to nucleons which peak around 0.7, restricting values of $R_{1.4M_{\odot}}$ to a reduced range \gtrapprox 13 km. The correlation between the slope of symmetry energy L_{sym} and radius of $1.4M_{\odot}$ NS is also lower than in the nucleonic case. A correlation between L_{sym} and $R_{1.4M_{\odot}}$ was reported in several articles in the literature [96, 97, 98, 99], although recent articles find $R_{1.4M_{\odot}}$ to be nearly independent of L_{sym} [69, 64]. Finally, the astrophysical observables studied in this work (mass, radius, tidal deformability) do not seem to provide correlations with hyperon potentials or the isovector coupling parameter y. However one must note that this is not generic for all astrophysical observables. One has to look for other observables, which are sensitive to the hyperon content in the NS interior, such as r-modes, cooling, thermal evolution etc (see e.g. [100]).

In another recent work [59], a Bayesian inference of the NS EoS was performed within the RMF model using astrophysical and nuclear saturation data. Using a selected class of nucleonic models with five empirical parameters and exploring different types of priors, they reported that the EoSs with the largest evidence were the ones featuring a strong reduction of the nucleon effective mass. However, the major drawback of this model was the omission of interaction terms (Λ_{ω} in our work) in the Lagrangian, due to

which other saturation parameters such as symmetry energy or its slope were not included. A preliminary investigation of the effect of hyperons was also performed by switching on only the Λ hyperon, with a fixed potential depth and coupling constants. However the effect of the other baryons of the octet and variation of the couplings as well as their correlations with other nuclear saturation parameters or NS observables was unexplored.

Another recent study [58] used Bayesian statistics to combine low density nuclear physics data, such as the ab-initio χ EFT predictions and the isoscalar giant monopole resonance, with astrophysical NS data, within the "metamodel" approach for the dense matter EoS. The posterior probability distribution functions were marginalized over several higher order nuclear empirical parameters (L_{sym} , K_{sym} , Q_{sat} , Q_{sym}), and observational quantities such as radius of $1.4M_{\odot}$ NS. This study also explored correlations among $L_{sym}-K_{sym}$ and $K_{sat}-Q_{sym}$ parameters, and reported marked tension between astrophysical and nuclear physics constraints. Some other work [43] combined laboratory experiments and NS astrophysical observation using Bayesian statistics along with the LIGO/Virgo and NICER observations within a hybrid nuclear+piecewise polytrope (PP) EoS parameterization. This work reported a very weak correlation between L_{sym} and $R_{1.4M_{\odot}}$. Recently Huth et al. [101] used a Bayesian inference technique to analyse the nuclear EoS and NS properties, combining data from heavy-ion collisions (FOPI [5] and ASY-EOS [6] experiments, EoS constraint for symmetric nuclear matter [102]), microscopic χEFT calculations and multi-messenger information from NICER and XMM Newton missions, as well as GW data and the associated kilonova AT2017gfo9. The study concluded that HIC constraints to be in excellent agreement with NICER observations. However, hyperons were not considered in the above investigations.

5.3 Limitations and future directions

In this work, the correlations between nuclear and hypernuclear parameters and NS astrophysical observables have been explored within the framework of the Relativistic Mean Field model. Although the advantage of this realistic phenomenological model is that, unlike polytropic or parametrized EoSs, the results provide important understanding of the underlying nuclear physics, it however remains to be established whether such physical correlations are also found in other realistic EoS models in order to generalise the results of this investigation. It would be interesting for example to see whether the conclusions would still hold for a Lagrangian with density-dependent couplings. Such possibilities will be addressed in a forthcoming publication. We recall here that the constraints from heavy-ion data are model-dependent and should therefore be treated on a different footing than astrophysical constraints and their implications on the results discussed with a word of caution.

In future, improved measurements of hyperon potentials in hypernuclear experiments, such as GSI in Germany, JLAB in USA and J-PARC in Japan [100], will reduce the uncertainties in the hyperon-nucleon and hyperon-hyperon coupling strengths. With the advent of multi-messenger astronomy, new upcoming observations of NS properties will also help to provide more stringent constraints on the dense matter EoS in NSs.

CONFLICT OF INTEREST STATEMENT

The authors declare that the research was conducted in the absence of any commercial or financial relationships that could be construed as a potential conflict of interest.

AUTHOR CONTRIBUTIONS

S.G. and B.-K.P. have contributed equally to this work and share first authorship. D.C. and J.S.-B. share senior authorship and contributed to the conception of the study. D.C. is the corresponding author of this article. Both S.G. and B.-K. P. performed the theoretical, numerical and statistical analysis. D.C. wrote the first draft, S.G. and B.-K.P. wrote sections of the manuscript. All authors contributed to manuscript revision, read, and approved the submitted version.

ACKNOWLEDGMENTS

D.C. is grateful to the hospitality of the Institut für theoretische Physik, J. W. Goethe Universität Frankfurt, Germany, where this work was carried out within the collaborative project "Astrophysical constraints for hyperons in neutron stars". S. G. B.K.P. and D.C. acknowledge usage of the IUCAA HPC computing facility for the numerical calculations.

FUNDING

This work was supported by the Deutsche Forschungsgemeinschaft (DFG, German Research Foundation) through the CRC-TR 211 'Strong-interaction matter under extreme conditions' – project number 315477589 – TRR 211.

REFERENCES

- [1] Baym G, Hatsuda T, Kojo T, Powell PD, Song Y, Takatsuka T. From hadrons to quarks in neutron stars: a review. *Reports on Progress in Physics* **81** (2018) 056902. doi:10.1088/1361-6633/aaae14.
- [2] David B, Alexander A, Alexandra F, Hovik G (Universe) (2020). doi:10.3390/books978-3-03921-959-9.
- [3] Lattimer JM. Introduction to neutron stars. *AIP Conference Proceedings* **1645** (2015) 61–78. doi:10.1063/1.4909560.
- [4] Gandolfi S, Gezerlis A, Carlson J. Neutron matter from low to high density. *Annual Review of Nuclear and Particle Science* **65** (2015) 303–328. doi:10.1146/annurev-nucl-102014-021957.
- [5] Le Fèvre A, Leifels Y, Reisdorf W, Aichelin J, Hartnack C. Constraining the nuclear matter equation of state around twice saturation density. *Nuclear Physics A* **945** (2016) 112–133. doi:https://doi.org/10.1016/j.nuclphysa.2015.09.015.
- [6] Russotto P, Gannon S, Kupny S, Lasko P, Acosta L, Adamczyk M, et al. Results of the asy-eos experiment at gsi: The symmetry energy at suprasaturation density. *Physical Review C* **94** (2016). doi:10.1103/physrevc.94.034608.
- [7] Inoue T. Hyperon single-particle potentials from QCD on lattice. *PoS* **INPC2016** (2016) 277. doi:10.22323/1.281.0277.
- [8] Inoue T. Hyperon Forces from QCD and Their Applications. *JPS Conf. Proc.* **26** (2019) 023018. doi:10.7566/JPSCP.26.023018.
- [9] Fabbietti L, Sarti VM, Doce OV. Study of the strong interaction among hadrons with correlations at the LHC. *Ann. Rev. Nucl. Part. Sci.* **71** (2021) 377–402. doi:10.1146/annurev-nucl-102419-034438.
- [10] Glendenning N. Compact Stars: Nuclear Physics, Particle Physics and General Relativity. Astronomy and Astrophysics Library (Springer New York) (2012).
- [11] Lattimer JM, Prakash M. The physics of neutron stars. *Science* **304** (2004) 536–542. doi:10.1126/science.1090720.

- [12] Oertel M, Hempel M, Klähn T, Typel S. Equations of state for supernovae and compact stars. *Rev. Mod. Phys.* **89** (2017) 015007. doi:10.1103/RevModPhys.89.015007.
- [13] Lattimer JM. The nuclear equation of state and neutron star masses. *Annual Review of Nuclear and Particle Science* **62** (2012) 485–515. doi:10.1146/annurev-nucl-102711-095018.
- [14] Stone J, Reinhard PG. The skyrme interaction in finite nuclei and nuclear matter. *Progress in Particle and Nuclear Physics* **58** (2007) 587–657. doi:10.1016/j.ppnp.2006.07.001.
- [15] Vautherin D, Brink DM. Hartree-fock calculations with skyrme's interaction. i. spherical nuclei. *Phys. Rev. C* **5** (1972) 626–647. doi:10.1103/PhysRevC.5.626.
- [16] Dutra M, Lourenço O, Sá Martins JS, Delfino A, Stone JR, Stevenson PD. Skyrme interaction and nuclear matter constraints. *Phys. Rev. C* **85** (2012) 035201. doi:10.1103/PhysRevC.85.035201.
- [17] Serot BD, Walecka JD. Relativistic nuclear many body theory. *Rec. Prog. Many Body Theor.* **3** (1992) 49–92. doi:10.1007/978-1-4615-3466-2_5.
- [18] Serot BD, Walecka JD. Recent progress in quantum hadrodynamics. *International Journal of Modern Physics E* **06** (1997) 515–631. doi:10.1142/s0218301397000299.
- [19] Demorest PB, Pennucci T, Ransom SM, Roberts MSE, Hessels JWT. A two-solar-mass neutron star measured using shapiro delay. *Nature* **467** (2010) 1081–1083. doi:10.1038/nature09466.
- [20] Antoniadis J, Freire PCC, Wex N, Tauris TM, Lynch RS, van Kerkwijk MH, et al. A massive pulsar in a compact relativistic binary. *Science* **340** (2013) 1233232–1233232. doi:10.1126/science.1233232.
- [21] Thorsett SE, Chakrabarty D. Neutron star mass measurements. i. radio pulsars. *The Astrophysical Journal* **512** (1999) 288–299. doi:10.1086/306742.
- [22] Özel F, Baym G, Güver T. Astrophysical measurement of the equation of state of neutron star matter. *Phys. Rev. D* **82** (2010) 101301. doi:10.1103/PhysRevD.82.101301.
- [23] Steiner AW, Lattimer JM, Brown EF. The neutron star mass-radius relation and the equation of state of dense matter. *The Astrophysical Journal* **765** (2013) L5. doi:10.1088/2041-8205/765/1/15.
- [24] Guillot S, Servillat M, Webb NA, Rutledge RE. Measurement of the radius of neutron stars with high signal-to-noise quiescent low-mass x-ray binaries in globular clusters. *The Astrophysical Journal* **772** (2013) 7. doi:10.1088/0004-637x/772/1/7.
- [25] Arzoumanian Z, Gendreau KC, Baker CL, Cazeau T, Hestnes P, Kellogg JW, et al. The neutron star interior composition explorer (NICER): mission definition. Takahashi T, den Herder JWA, Bautz M, editors, Space Telescopes and Instrumentation 2014: Ultraviolet to Gamma Ray (2014), Society of Photo-Optical Instrumentation Engineers (SPIE) Conference Series, vol. 9144, 914420. doi:10.1117/12.2056811.
- [26] Miller MC, Lamb FK, Dittmann AJ, Bogdanov S, Arzoumanian Z, Gendreau KC, et al. Psr j0030+0451 mass and radius from nicer data and implications for the properties of neutron star matter. *The Astrophysical Journal* **887** (2019) L24. doi:10.3847/2041-8213/ab50c5.
- [27] Riley TE, Watts AL, Bogdanov S, Ray PS, Ludlam RM, Guillot S, et al. A nicer view of psr j0030+0451: Millisecond pulsar parameter estimation. *The Astrophysical Journal* **887** (2019) L21. doi:10.3847/2041-8213/ab481c.
- [28] Miller MC, Lamb FK, Dittmann AJ, Bogdanov S, Arzoumanian Z, Gendreau KC, et al. The radius of psr j0740+6620 from nicer and xmm-newton data. *The Astrophysical Journal Letters* **918** (2021) L28. doi:10.3847/2041-8213/ac089b.
- [29] Riley TE, Watts AL, Ray PS, Bogdanov S, Guillot S, Morsink SM, et al. A nicer view of the massive pulsar psr j0740+6620 informed by radio timing and xmm-newton spectroscopy. *The Astrophysical Journal Letters* **918** (2021) L27. doi:10.3847/2041-8213/ac0a81.

- [30] Abbott BP, et al. Gw170817: Observation of gravitational waves from a binary neutron star inspiral. *Phys. Rev. Lett.* **119** (2017) 161101. doi:10.1103/PhysRevLett.119.161101.
- [31] Abbott R, Abbott TD, Abraham S, Acernese F, Ackley K, Adams A, et al. Observation of gravitational waves from two neutron star–black hole coalescences. *The Astrophysical Journal Letters* **915** (2021) L5. doi:10.3847/2041-8213/ac082e.
- [32] Abbott BP, Abbott R, Abbott TD, Abraham S, et al FA. GW190425: Observation of a compact binary coalescence with total mass $\sim 3.4~\text{m}\odot$. *The Astrophysical Journal Letters* **892** (2020) L3. doi:10.3847/2041-8213/ab75f5.
- [33] Aasi J, Abbott BP, Abbott R, Abbott T, Abernathy MR, Ackley K, et al. Advanced LIGO. *Classical and Quantum Gravity* **32** (2015) 074001. doi:10.1088/0264-9381/32/7/074001.
- [34] Acernese F, Agathos M, Agatsuma K, Aisa D, et al. Advanced virgo: a second-generation interferometric gravitational wave detector. *Classical and Quantum Gravity* **32** (2014) 024001. doi:10.1088/0264-9381/32/2/024001.
- [35] Abbott BP, et al. Gw170817: Measurements of neutron star radii and equation of state. *Phys. Rev. Lett.* **121** (2018) 161101. doi:10.1103/PhysRevLett.121.161101.
- [36] Abbott B, Abbott R, Abbott T, Acernese F, Ackley K, Adams C, et al. Properties of the binary neutron star merger gw170817. *Phys. Rev. X* **9** (2019) 011001. doi:10.1103/PhysRevX.9.011001.
- [37] Most ER, Weih LR, Rezzolla L, Schaffner-Bielich J. New constraints on radii and tidal deformabilities of neutron stars from gw170817. *Phys. Rev. Lett.* **120** (2018) 261103. doi:10.1103/PhysRevLett.120. 261103.
- [38] Annala E, Gorda T, Kurkela A, Vuorinen A. Gravitational-wave constraints on the neutron-star-matter equation of state. *Phys. Rev. Lett.* **120** (2018) 172703. doi:10.1103/PhysRevLett.120.172703.
- [39] Pang PTH, Tews I, Coughlin MW, Bulla M, Van Den Broeck C, Dietrich T. Nuclear Physics Multimessenger Astrophysics Constraints on the Neutron Star Equation of State: Adding NICER's PSR J0740+6620 Measurement. *Astro. phys. journal* **922** (2021) 14. doi:10.3847/1538-4357/ac19ab.
- [40] Coughlin MW, Dietrich T, Margalit B, Metzger BD. Multimessenger bayesian parameter inference of a binary neutron star merger. *Monthly Notices of the Royal Astronomical Society: Letters* **489** (2019) L91–L96. doi:10.1093/mnrasl/slz133.
- [41] Biswas B, Char P, Nandi R, Bose S. Towards mitigation of apparent tension between nuclear physics and astrophysical observations by improved modeling of neutron star matter. *Phys. Rev. D* **103** (2021) 103015. doi:10.1103/PhysRevD.103.103015.
- [42] Biswas B. Impact of PREX-II and Combined Radio/NICER/XMM-Newton's Mass-radius Measurement of PSR J0740+6620 on the Dense-matter Equation of State. *Astrophys. J.* **921** (2021) 63. doi:10.3847/1538-4357/ac1c72.
- [43] Biswas B. Bayesian model-selection of neutron star equation of state using multi-messenger observations. *arXiv e-prints* (2021) arXiv:2106.02644.
- [44] Dietrich T, Coughlin MW, Pang PTH, Bulla M, Heinzel J, Issa L, et al. Multimessenger constraints on the neutron-star equation of state and the hubble constant. *Science* **370** (2020) 1450–1453. doi:10.1126/science.abb4317.
- [45] O'Boyle MF, Markakis C, Stergioulas N, Read JS. Parametrized equation of state for neutron star matter with continuous sound speed. *Phys. Rev. D* **102** (2020) 083027. doi:10.1103/PhysRevD.102. 083027.
- [46] Capano CD, Tews I, Brown SM, Margalit B, De S, Kumar S, et al. Stringent constraints on neutron-star radii from multimessenger observations and nuclear theory. *Nature Astronomy* **4** (2020) 625–632. doi:10.1038/s41550-020-1014-6.

- [47] Tews I, Margueron J, Reddy S. Critical examination of constraints on the equation of state of dense matter obtained from gw170817. *Phys. Rev. C* **98** (2018) 045804. doi:10.1103/PhysRevC.98.045804.
- [48] Tews I, Margueron J, Reddy S. Constraining the properties of dense matter and neutron stars by combining nuclear physics and gravitational waves from gw170817. *AIP Conference Proceedings* **2127** (2019) 020009. doi:10.1063/1.5117799.
- [49] Tews I, Margueron J, Reddy S. Confronting gravitational-wave observations with modern nuclear physics constraints. *The European Physical Journal A* **55** (2019). doi:10.1140/epja/i2019-12774-6.
- [50] Gandolfi S, Lippuner J, Steiner AW, Tews I, Du X, Al-Mamun M. From the microscopic to the macroscopic world: from nucleons to neutron stars. *Journal of Physics G: Nuclear and Particle Physics* **46** (2019) 103001. doi:10.1088/1361-6471/ab29b3.
- [51] Hebeler K, Lattimer JM, Pethick CJ, Schwenk A. Equation of state and neutron star properties constrained by nuclear physics and observation. *The Astrophysical Journal* **773** (2013) 11. doi:10. 1088/0004-637x/773/1/11.
- [52] Read JS, Lackey BD, Owen BJ, Friedman JL. Constraints on a phenomenologically parametrized neutron-star equation of state. *Physical Review D* **79** (2009). doi:10.1103/physrevd.79.124032.
- [53] Gamba R, Read JS, Wade LE. The impact of the crust equation of state on the analysis of GW170817. *Classical and Quantum Gravity* **37** (2019) 025008. doi:10.1088/1361-6382/ab5ba4.
- [54] Fasano M, Abdelsalhin T, Maselli A, Ferrari V. Constraining the neutron star equation of state using multiband independent measurements of radii and tidal deformabilities. *Phys. Rev. Lett.* **123** (2019) 141101. doi:10.1103/PhysRevLett.123.141101.
- [55] Lindblom L. Causal representations of neutron-star equations of state. *Phys. Rev. D* **97** (2018) 123019. doi:10.1103/PhysRevD.97.123019.
- [56] Greif SK, Raaijmakers G, Hebeler K, Schwenk A, Watts AL. Equation of state sensitivities when inferring neutron star and dense matter properties. *Monthly Notices of the Royal Astronomical Society* **485** (2019) 5363–5376. doi:10.1093/mnras/stz654.
- [57] Landry P, Essick R, Chatziioannou K. Nonparametric constraints on neutron star matter with existing and upcoming gravitational wave and pulsar observations. *Phys. Rev. D* **101** (2020) 123007. doi:10.1103/PhysRevD.101.123007.
- [58] Güven H, Bozkurt K, Khan E, Margueron J. Multimessenger and multiphysics bayesian inference for the gw170817 binary neutron star merger. *Phys. Rev. C* **102** (2020) 015805. doi:10.1103/PhysRevC. 102.015805.
- [59] Traversi S, Char P, Pagliara G. Bayesian inference of dense matter equation of state within relativistic mean field models using astrophysical measurements. *The Astrophysical Journal* **897** (2020) 165. doi:10.3847/1538-4357/ab99c1.
- [60] Zhang NB, Li BA. Implications of the mass $m=2.17^{+0.11}_{-0.10}~{\rm m}_{\odot}{\rm of}$ psr j0740+6620 on the equation of state of super-dense neutron-rich nuclear matter. The Astrophysical Journal 879 (2019) 99. doi:10.3847/1538-4357/ab24cb.
- [61] Xie WJ, Li BA. Bayesian inference of high-density nuclear symmetry energy from radii of canonical neutron stars. *The Astrophysical Journal* **883** (2019) 174. doi:10.3847/1538-4357/ab3f37.
- [62] Carson Z, Steiner AW, Yagi K. Constraining nuclear matter parameters with gw170817. *Phys. Rev.* D 99 (2019) 043010. doi:10.1103/PhysRevD.99.043010.
- [63] Zimmerman J, Carson Z, Schumacher K, Steiner AW, Yagi K. Measuring Nuclear Matter Parameters with NICER and LIGO/Virgo. *arXiv e-prints* (2020) arXiv:2002.03210.
- [64] Ghosh S, Chatterjee D, Schaffner-Bielich J. Imposing multi-physics constraints at different densities on the Neutron Star Equation of State. *arXiv e-prints* (2021) arXiv:2107.09371.

- [65] Dexheimer V, Noronha J, Noronha-Hostler J, Yunes N, Ratti C. Future physics perspectives on the equation of state from heavy ion collisions to neutron stars. *Journal of Physics G: Nuclear and Particle Physics* **48** (2021) 073001. doi:10.1088/1361-6471/abe104.
- [66] Tsang CY, Tsang MB, Danielewicz P, Lynch WG, Fattoyev FJ. Constraining neutron-star equation of state using heavy-ion collisions. *arXiv e-prints* (2018) arXiv:1807.06571.
- [67] Weissenborn S, Chatterjee D, Schaffner-Bielich J. Hyperons and massive neutron stars: The role of hyperon potentials. *Nuclear Physics A* **881** (2012) 62 77. doi:https://doi.org/10.1016/j.nuclphysa. 2012.02.012.
- [68] Pradhan BK, Chatterjee D. Effect of hyperons on *f*-mode oscillations in neutron stars. *Phys. Rev. C* **103** (2021) 035810. doi:10.1103/PhysRevC.103.035810.
- [69] Hornick N, Tolos L, Zacchi A, Christian JE, Schaffner-Bielich J. Relativistic parameterizations of neutron matter and implications for neutron stars. *Phys. Rev. C* 98 (2018) 065804. doi:10.1103/ PhysRevC.98.065804.
- [70] Chen WC, Piekarewicz J. Building relativistic mean field models for finite nuclei and neutron stars. *Phys. Rev. C* **90** (2014) 044305. doi:10.1103/PhysRevC.90.044305.
- [71] Millener DJ, Dover CB, Gal A. Λ-nucleus single-particle potentials. *Phys. Rev. C* **38** (1988) 2700–2708. doi:10.1103/PhysRevC.38.2700.
- [72] Schaffner J, Greiner C, Stöcker H. Metastable exotic multihypernuclear objects. *Phys. Rev. C* **46** (1992) 322–329. doi:10.1103/PhysRevC.46.322.
- [73] Friedman E, Gal A. In-medium nuclear interactions of low-energy hadrons. *Physics Reports* **452** (2007) 89–153. doi:10.1016/j.physrep.2007.08.002.
- [74] Schaffner-Bielich J, Gal A. Properties of strange hadronic matter in bulk and in finite systems. *Phys. Rev. C* **62** (2000) 034311. doi:10.1103/PhysRevC.62.034311.
- [75] Mareš J, Friedman E, Gal A, Jenning B. Constraints on σ -nucleus dynamics from dirac phenomenology of σ^- atoms. *Nuclear Physics A* **594** (1995) 311–324. doi:https://doi.org/10. 1016/0375-9474(95)00358-8.
- [76] Fukuda T, Higashi A, Matsuyama Y, Nagoshi C, Nakano J, Sekimoto M, et al. Cascade hypernuclei in the (K⁻,K⁺) reaction on ¹²C. *Phy. Rev. C* **58** (1998) 1306–1309. doi:10.1103/PhysRevC.58.1306.
- [77] Khaustov P, Alburger DE, Barnes PD, Bassalleck B, Berdoz AR, Biglan A, et al. Evidence of Ξ hypernuclear production in the ${}^{12}\mathrm{C}(K^-,K^+)^{12}_{\Xi}\mathrm{Be}$ reaction. *Phys. Rev. C* **61** (2000) 054603. doi:10.1103/PhysRevC.61.054603.
- [78] Schaffner J, Dover CB, Gal A, Greiner C, Stöcker H. Strange hadronic matter. *Phys. Rev. Lett.* **71** (1993) 1328–1331. doi:10.1103/PhysRevLett.71.1328.
- [79] Schaffner-Bielich J. *Compact Star Physics* (Cambridge University Press) (2020). doi:10.1017/9781316848357.
- [80] Hinderer T. Tidal love numbers of neutron stars. *The Astrophysical Journal* **677** (2008) 1216–1220. doi:10.1086/533487.
- [81] Flanagan EE, Hinderer T. Constraining neutron-star tidal love numbers with gravitational-wave detectors. *Phys. Rev. D* **77** (2008) 021502. doi:10.1103/PhysRevD.77.021502.
- [82] Yagi K, Yunes N. I-love-q relations in neutron stars and their applications to astrophysics, gravitational waves, and fundamental physics. *Phys. Rev. D* **88** (2013) 023009. doi:10.1103/PhysRevD.88.023009.
- [83] Hinderer T, Lackey BD, Lang RN, Read JS. Tidal deformability of neutron stars with realistic equations of state and their gravitational wave signatures in binary inspiral. *Phys. Rev. D* **81** (2010) 123016. doi:10.1103/PhysRevD.81.123016.

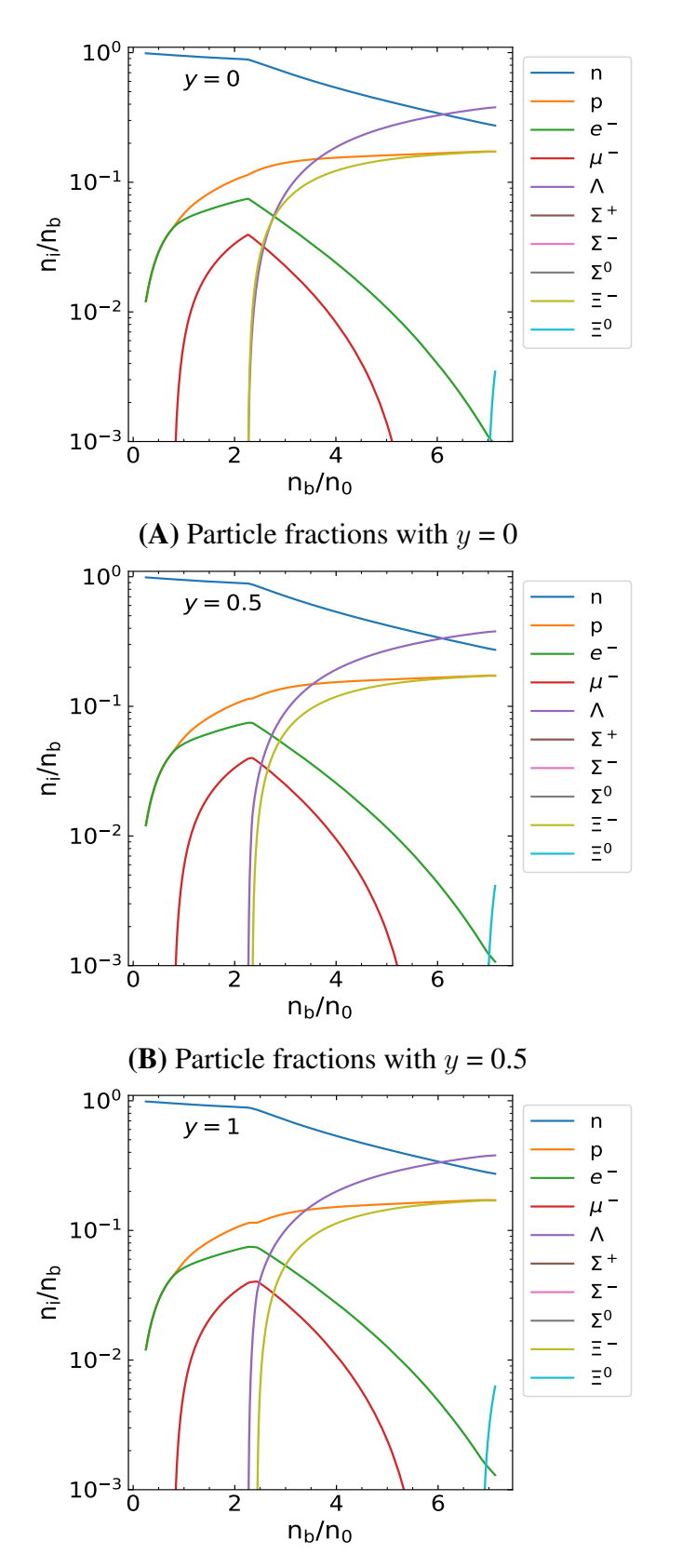
- [84] Miller MC, Chirenti C, Lamb FK. Constraining the equation of state of high-density cold matter using nuclear and astronomical measurements. *The Astrophysical Journal* **888** (2019) 12. doi:10. 3847/1538-4357/ab4ef9.
- [85] Annala E, Gorda T, Kurkela A, Nättilä J, Vuorinen A. Evidence for quark-matter cores in massive neutron stars. *Nature Physics* **16** (2020) 907–910. doi:10.1038/s41567-020-0914-9.
- [86] Annala E, Gorda T, Katerini E, Kurkela A, Nättilä J, Paschalidis V, et al. Multimessenger constraints for ultra-dense matter. *arXiv e-prints* (2021) arXiv:2105.05132.
- [87] Wei, Jin-Biao, Lu, Jia-Jing, Burgio, G F, Li, Zeng-Hua, Schulze, H-J. Are nuclear matter properties correlated to neutron star observables? *Eur. Phys. J. A* **56** (2020) 63. doi:10.1140/epja/s10050-020-00058-3.
- [88] Drischler C, Carbone A, Hebeler K, Schwenk A. Neutron matter from chiral two- and three-nucleon calculations up to N³LO. *Phys. Rev. C* **94** (2016) 054307. doi:10.1103/PhysRevC.94.054307.
- [89] Drischler C, Furnstahl RJ, Melendez JA, Phillips DR. How well do we know the neutron-matter equation of state at the densities inside neutron stars? a bayesian approach with correlated uncertainties. *Phys. Rev. Lett.* **125** (2020) 202702. doi:10.1103/PhysRevLett.125.202702.
- [90] Drischler C, Hebeler K, Schwenk A. Chiral interactions up to next-to-next-to-next-to-leading order and nuclear saturation. *Phys. Rev. Lett.* **122** (2019) 042501. doi:10.1103/PhysRevLett.122.042501.
- [91] Fonseca E, et al. Refined Mass and Geometric Measurements of the High-mass PSR J0740+6620. *Astrophys. J. Lett.* **915** (2021) L12. doi:10.3847/2041-8213/ac03b8.
- [92] Tong H, Zhao P, Meng J. Symmetry energy at supra-saturation densities via the gravitational waves from gw170817. *Phys. Rev. C* **101** (2020) 035802. doi:10.1103/PhysRevC.101.035802.
- [93] Hartnack C, Oeschler H, Aichelin J. Hadronic matter is soft. *Phys. Rev. Lett.* **96** (2006) 012302. doi:10.1103/PhysRevLett.96.012302.
- [94] Fuchs C, Faessler A, Zabrodin E, Zheng YM. Probing the nuclear equation of state by K^+ production in heavy-ion collisions. *Phys. Rev. Lett.* **86** (2001) 1974–1977. doi:10.1103/PhysRevLett.86.1974.
- [95] Kirch W, editor. *Pearson's Correlation Coefficient* (Dordrecht: Springer Netherlands) (2008), 1090–1091. doi:10.1007/978-1-4020-5614-7_2569.
- [96] Fattoyev FJ, Carvajal J, Newton WG, Li BA. Constraining the high-density behavior of the nuclear symmetry energy with the tidal polarizability of neutron stars. *Phys. Rev. C* **87** (2013) 015806. doi:10.1103/PhysRevC.87.015806.
- [97] Alam N, Agrawal BK, Fortin M, Pais H, Providência C, Raduta AR, et al. Strong correlations of neutron star radii with the slopes of nuclear matter incompressibility and symmetry energy at saturation. *Phys. Rev. C* **94** (2016) 052801. doi:10.1103/PhysRevC.94.052801.
- [98] Zhu ZY, Zhou EP, Li A. Neutron star equation of state from the quark level in light of gw170817. *The Astrophysical Journal* **862** (2018) 98. doi:10.3847/1538-4357/aacc28.
- [99] Lim Y, Holt JW. Neutron star tidal deformabilities constrained by nuclear theory and experiment. *Phys. Rev. Lett.* **121** (2018) 062701. doi:10.1103/PhysRevLett.121.062701.
- [100] Chatterjee D, Vidaña I. Do hyperons exist in the interior of neutron stars? *Eur. Phys. J.* **A52** (2016) 29. doi:10.1140/epja/i2016-16029-x.
- [101] Huth S, Pang PTH, Tews I, Dietrich T, Le Fèvre A, Schwenk A, et al. Constraining Neutron-Star Matter with Microscopic and Macroscopic Collisions. *arXiv e-prints* (2021) arXiv:2107.06229.
- [102] Danielewicz P, Lacey R, Lynch WG. Determination of the equation of state of dense matter. *Science* **298** (2002) 1592–1596. doi:10.1126/science.1078070.

TABLES

Table 1. Range (minimum and maximum values) of nuclear and hypernuclear parameters at saturation density used in this work. Masses of mesons and the nucleon are fixed as $m_\sigma=550~{\rm MeV},~{\rm m}_\omega=783~{\rm MeV},~{\rm m}_\rho=770~{\rm MeV},~{\rm m}_\phi=1020~{\rm MeV}$ and ${\rm m}_{\rm N}=939~{\rm MeV}.$

$n_0 \ (\text{fm}^{-3})$	$E_{\rm sat}$ (MeV)	(MeV)	E_{sym} (MeV)	$L_{ m sym}$ (MeV)	m^* (m_N)	U_{Λ} (MeV)	U_{Σ} (MeV)	U_{Ξ} (MeV)	y
0.14 0.17	-16.2 -15.8	200 300	28 34	40 70	0.55 0.75	-30 -30	0 30	-30 0	0

FIGURES



(C) Particle fractions with y given by SU(6) symmetry

Figure 1. Particle fractions for varying y parameter (isovector hyperon coupling). The nuclear and hyper nuclear parameters are fixed to, $m^* = 0.65 m_N$, $E_{sat} = -16$ MeV, $K_{sat} = 240$ MeV, $J_{sym} = 32$ MeV, $L_{sym} = 60$ MeV, $U_{\Lambda} = -30$ MeV, $U_{\Sigma} = +30$ MeV, $U_{\Xi} = -28$ MeV.

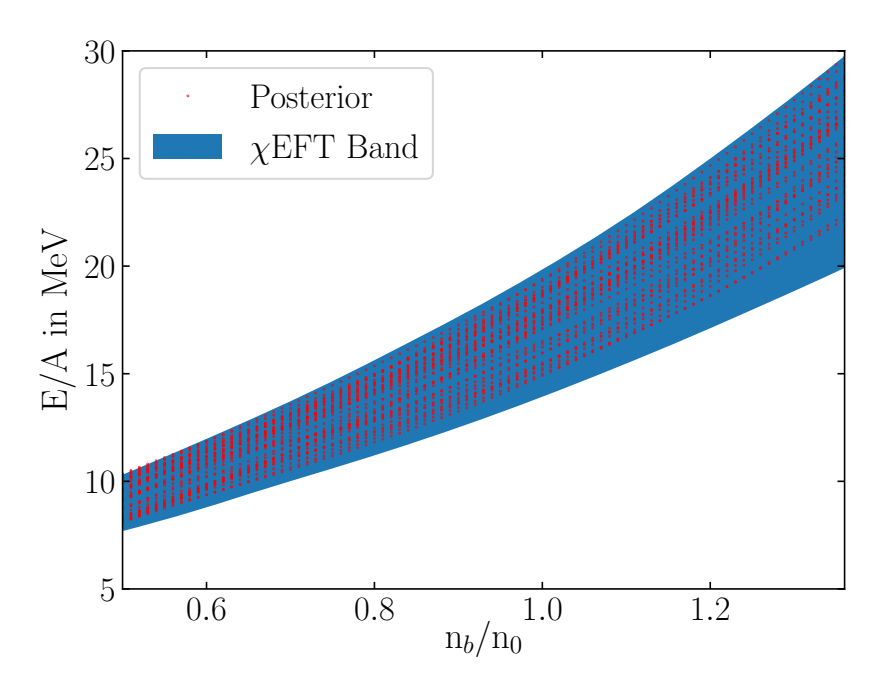
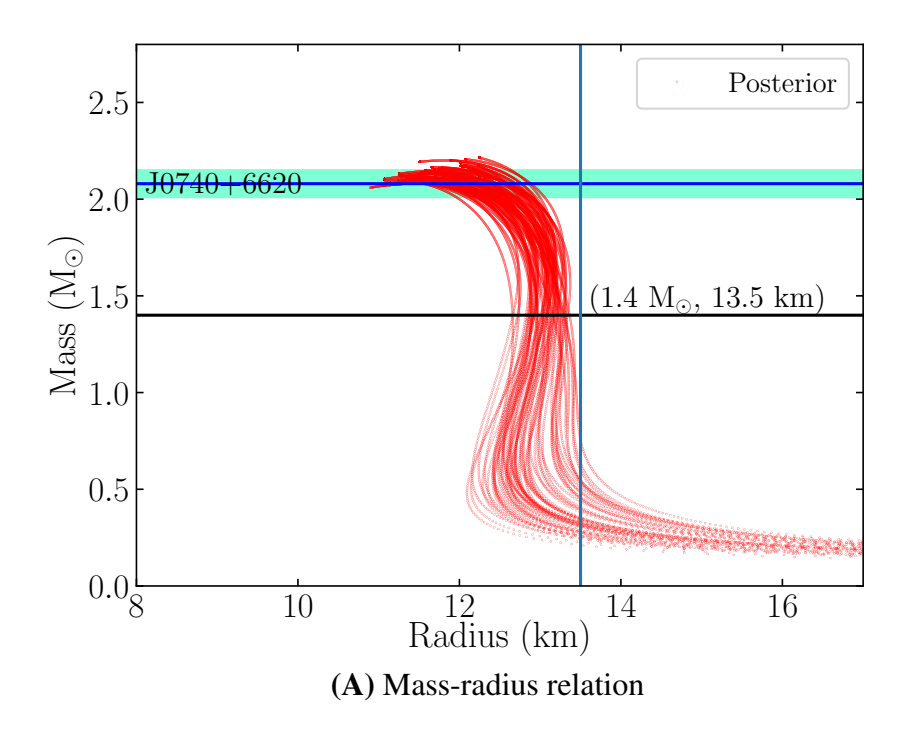


Figure 2. Binding energy E/A of posterior pure neutron matter EoSs as a function of normalized density n_b/n_0 allowed by chiral effective field theory (χ EFT) data [90].



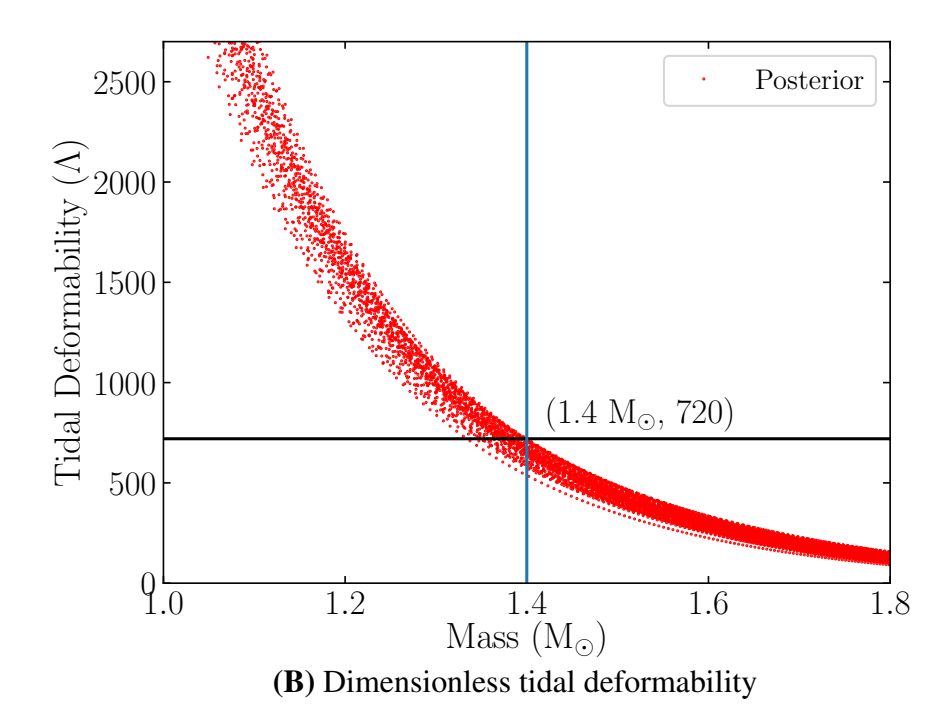


Figure 3. NS observables for the posterior hyperon EoSs after passing through χ EFT and NS observations filters. The light green band indicates the uncertainty in the measurement of maximum mass of PSR J0740+6620 [91]

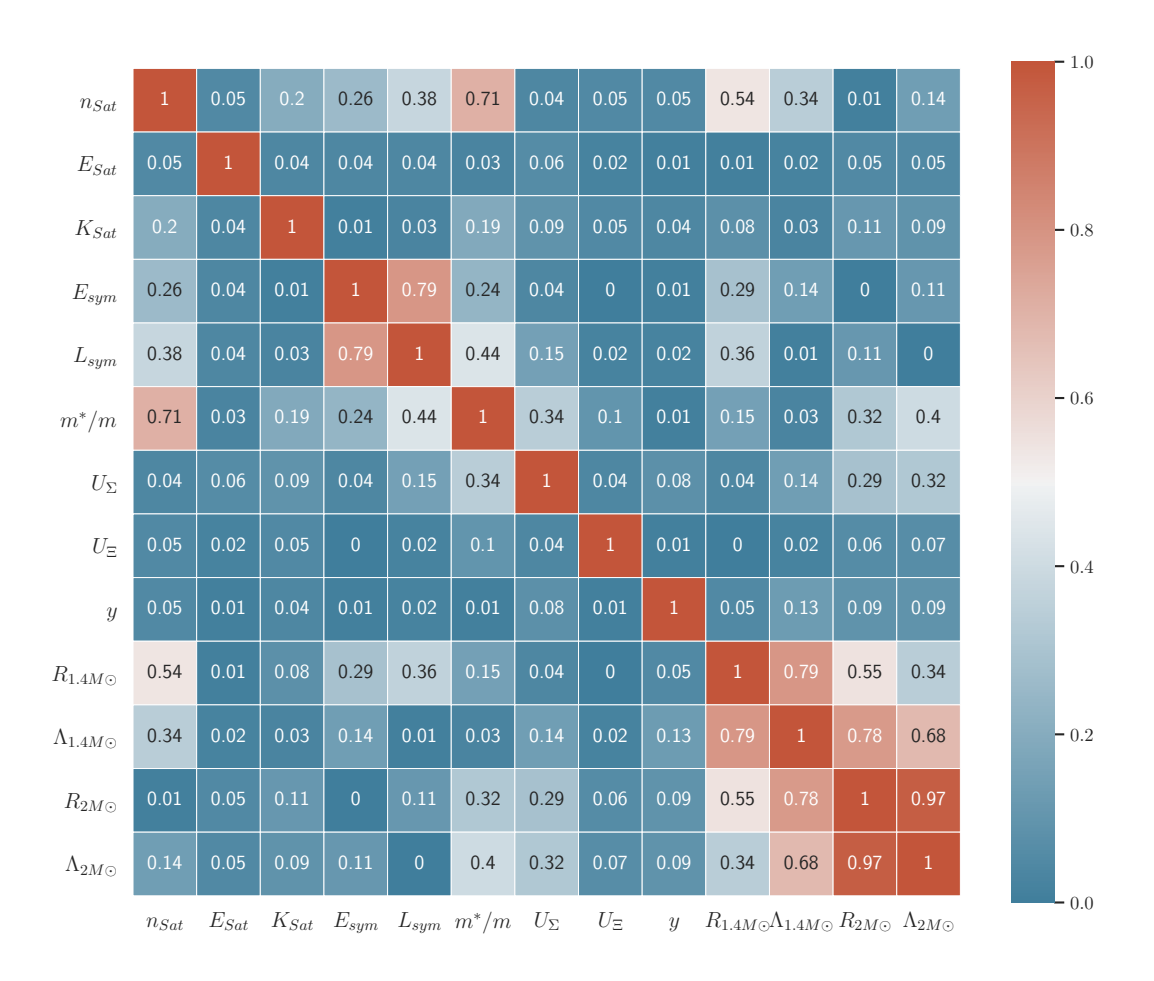


Figure 4. Posterior correlation matrix for variation of nuclear empirical parameters and NS observables, after application of the χ EFT and NS observations filter

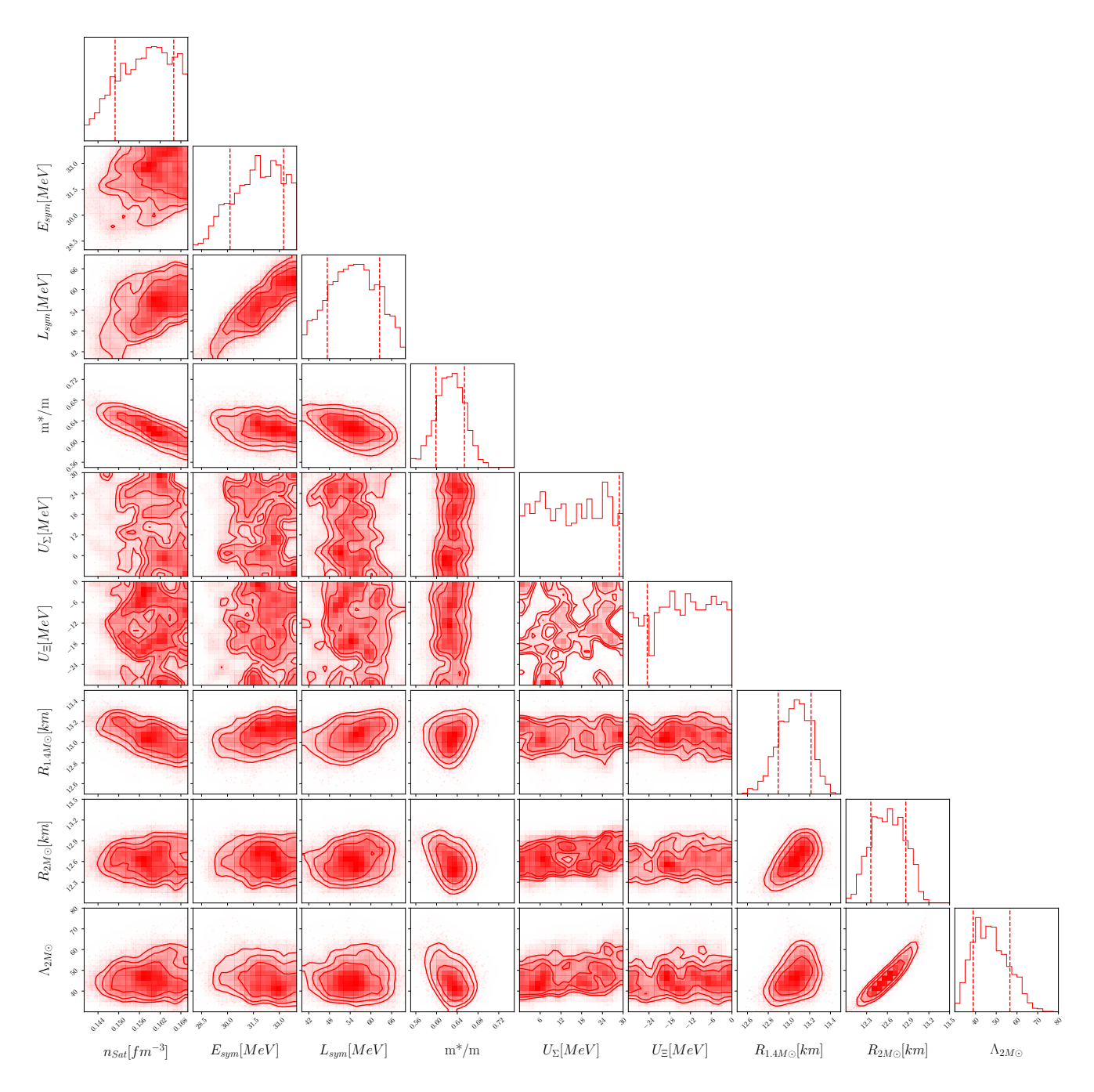


Figure 5. Posterior distributions of nuclear parameters and astrophysical observables after applying the $\chi \rm EFT$ and the astrophysical constraints.

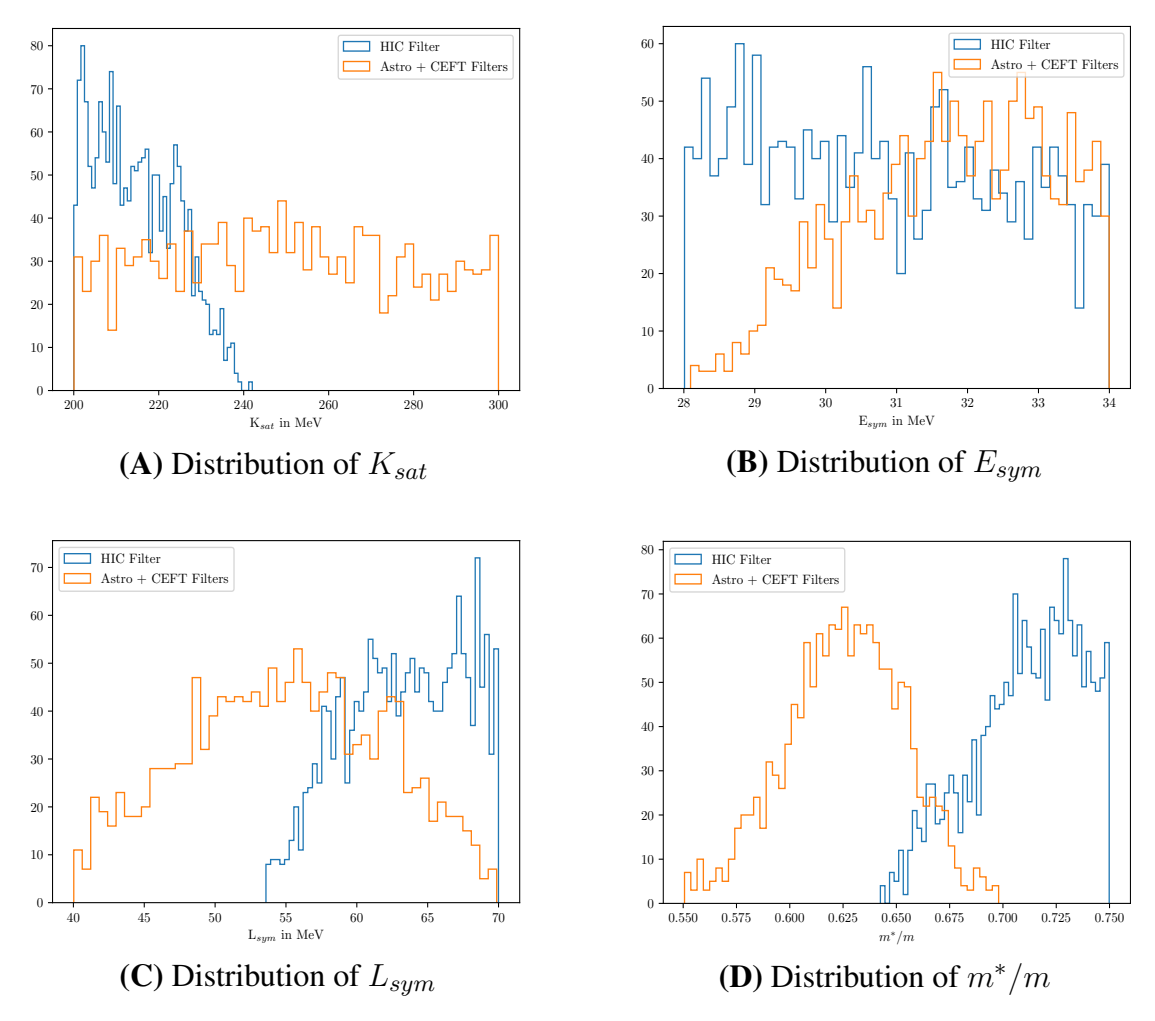


Figure 6. Distribution of some nuclear saturation parameters, after application of the HIC filters (KaoS, FOPI, ASY-EOS)

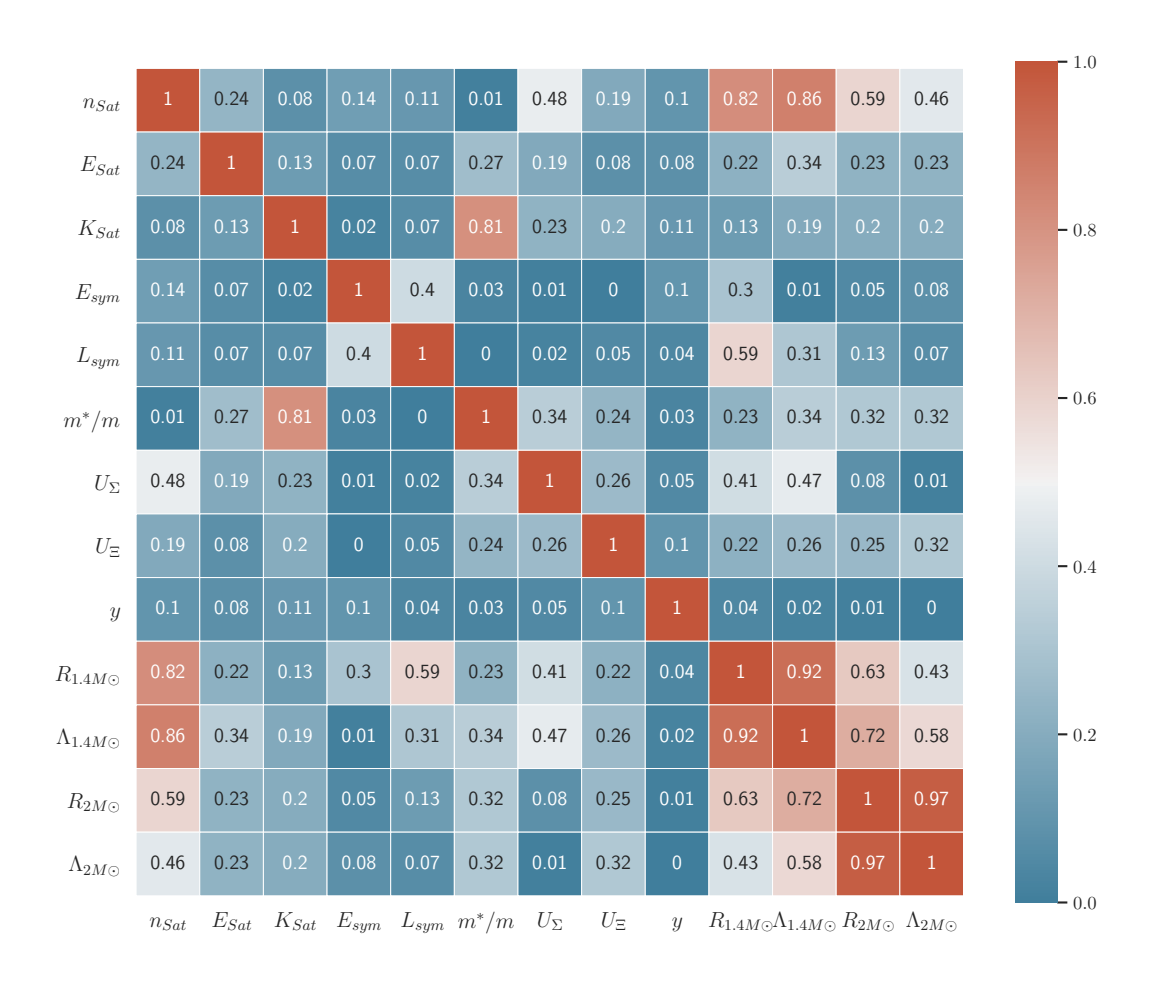


Figure 7. Posterior correlation matrix for variation of nuclear empirical parameters and NS observables, after application of the χ EFT, HIC and NS observations filters